

Temperature study of atmospheric-pressure plasma-enhanced spatial ALD of Al₂O₃ using infrared and optical emission spectroscopy

Citation for published version (APA):

Mione, M. A., Vandalon, V., Kessels, W. M. M., & Roozeboom, F. (2022). Temperature study of atmospheric-pressure plasma-enhanced spatial ALD of Al₂O₃ using infrared and optical emission spectroscopy. *Journal of Vacuum Science and Technology A*, 40(6), Article 062407. <https://doi.org/10.1116/6.0002158>

Document license:
CC BY

DOI:
[10.1116/6.0002158](https://doi.org/10.1116/6.0002158)

Document status and date:
Published: 04/11/2022

Document Version:
Publisher's PDF, also known as Version of Record (includes final page, issue and volume numbers)

Please check the document version of this publication:

- A submitted manuscript is the version of the article upon submission and before peer-review. There can be important differences between the submitted version and the official published version of record. People interested in the research are advised to contact the author for the final version of the publication, or visit the DOI to the publisher's website.
- The final author version and the galley proof are versions of the publication after peer review.
- The final published version features the final layout of the paper including the volume, issue and page numbers.

[Link to publication](#)

General rights

Copyright and moral rights for the publications made accessible in the public portal are retained by the authors and/or other copyright owners and it is a condition of accessing publications that users recognise and abide by the legal requirements associated with these rights.

- Users may download and print one copy of any publication from the public portal for the purpose of private study or research.
- You may not further distribute the material or use it for any profit-making activity or commercial gain
- You may freely distribute the URL identifying the publication in the public portal.

If the publication is distributed under the terms of Article 25fa of the Dutch Copyright Act, indicated by the "Taverne" license above, please follow below link for the End User Agreement:

www.tue.nl/taverne

Take down policy

If you believe that this document breaches copyright please contact us at:

openaccess@tue.nl

providing details and we will investigate your claim.

Temperature study of atmospheric-pressure plasma-enhanced spatial ALD of Al_2O_3 using infrared and optical emission spectroscopy

Cite as: J. Vac. Sci. Technol. A **40**, 062407 (2022); <https://doi.org/10.1116/6.0002158>

Submitted: 15 August 2022 • Accepted: 30 September 2022 • Published Online: 04 November 2022

 M. A. Mione,  V. Vandalon,  W. M. M. Kessels, et al.

COLLECTIONS

Paper published as part of the special topic on [Atomic Layer Deposition \(ALD\)](#)



View Online



Export Citation



CrossMark

ARTICLES YOU MAY BE INTERESTED IN

[Temperature dependence of on-off ratio and reverse recovery time in \$\text{NiO}/\beta\text{-Ga}_2\text{O}_3\$ heterojunction rectifiers](#)


Journal of Vacuum Science & Technology A **40**, 063407 (2022); <https://doi.org/10.1116/6.0002186>

[MOCVD growth and band offsets of \$\kappa\$ -phase \$\text{Ga}_2\text{O}_3\$ on c-plane sapphire, GaN- and AlN-on-sapphire, and \(100\) YSZ substrates](#)


Journal of Vacuum Science & Technology A **40**, 062704 (2022); <https://doi.org/10.1116/6.0002106>

[Diffusion-assisted molecular beam epitaxy of \$\text{CuCrO}_2\$ thin films](#)

Journal of Vacuum Science & Technology A **40**, 060401 (2022); <https://doi.org/10.1116/6.0002151>



HIDEN
ANALYTICAL



40 YEARS
1982 - 2022


Instruments for Advanced Science

- Knowledge,
- Experience,
- Expertise

Click to view our product catalogue


Contact Hiden Analytical for further details:
www.HidenAnalytical.com
info@hideninc.com

Gas Analysis




- ▶ dynamic measurement of reaction gas streams
- ▶ catalysis and thermal analysis
- ▶ molecular beam studies
- ▶ dissolved species probes
- ▶ fermentation, environmental and ecological studies

Surface Science




- ▶ UHVTPD
- ▶ SIMS
- ▶ end point detection in ion beam etch
- ▶ elemental imaging - surface mapping

Plasma Diagnostics



- ▶ plasma source characterization
- ▶ etch and deposition process reaction kinetic studies
- ▶ analysis of neutral and radical species

Vacuum Analysis



- ▶ partial pressure measurement and control of process gases
- ▶ reactive sputter process control
- ▶ vacuum diagnostics
- ▶ vacuum coating process monitoring



Temperature study of atmospheric-pressure plasma-enhanced spatial ALD of Al_2O_3 using infrared and optical emission spectroscopy

Cite as: J. Vac. Sci. Technol. A 40, 062407 (2022); doi: 10.1116/6.0002158

Submitted: 15 August 2022 · Accepted: 30 September 2022 ·

Published Online: 4 November 2022



M. A. Mione, V. Vandalon, W. M. M. Kessels, and F. Roozeboom

AFFILIATIONS

Department of Applied Physics, Eindhoven University of Technology, P.O. Box 513, 5600 MB Eindhoven, The Netherlands

Note: This paper is part of the 2023 Special Topic Collection on Atomic Layer Deposition (ALD).

^{a)}**Current address:** ASM International, Kapeldreef 75, 3001 Leuven, Belgium

^{b)}**Author to whom correspondence should be addressed:** w.m.m.kessels@tue.nl

^{c)}**Current address:** Faculty of Science and Technology, University Twente, P.O. Box 217, 7500 AE Enschede, The Netherlands

ABSTRACT

Atmospheric-pressure plasma-enhanced spatial atomic layer deposition (PE-s-ALD) is considered a promising technique for high-throughput and low-temperature deposition of ultrathin films for applications where volume and costs are particularly relevant. The number of atmospheric-pressure PE-s-ALD processes developed so far is rather limited, and the fundamental aspects of their growth mechanisms are largely unexplored. This work presents a study of the atmospheric-pressure PE-s-ALD process of Al_2O_3 using trimethylaluminum [TMA, $\text{Al}(\text{CH}_3)_3$] and Ar- O_2 plasma within the temperature range of 80–200 °C. Thin-film analysis revealed low impurity contents and a decreasing growth-per-cycle (GPC) with increasing temperature. The underlying chemistry of the process was studied with a combination of gas-phase infrared spectroscopy on the exhaust plasma gas and optical emission spectroscopy (OES) on the plasma zone. Among the chemical species formed in the plasma half-cycle, CO_2 , H_2O , CH_4 , and CH_2O were identified. The formation of these products confirms that the removal of CH_3 ligands during the plasma half-cycle occurs through two reaction pathways that have a different temperature dependences: (i) combustion reactions initiated by O_2 plasma species and leading to CO_2 and H_2O formation and (ii) thermal ALD-like reactions initiated by the H_2O molecules formed in pathway (i) and resulting in CH_4 production. With increasing temperature, the dehydroxylation of OH groups cause less TMA adsorption which leads to less CO_2 and H_2O from the combustion reactions in the plasma step. At the same time, the higher reactivity of H_2O at higher temperatures initiates more thermal ALD-like reactions, thus producing relatively more CH_4 . The CH_4 can also undergo further gas-phase reactions leading to the formation of CH_2O as was theoretically predicted. Another observation is that O_3 , which is naturally produced in the atmospheric-pressure O_2 plasma, decomposes at higher temperatures mainly due to an increase of gas-phase collisions. In addition to the new insights into the growth mechanism of atmospheric-pressure PE-s-ALD of Al_2O_3 , this work presents a method to study both the surface chemistry during spatial ALD to further extend our fundamental understanding of the method.

© 2022 Author(s). All article content, except where otherwise noted, is licensed under a Creative Commons Attribution (CC BY) license (<http://creativecommons.org/licenses/by/4.0/>). <https://doi.org/10.1116/6.0002158>

I. INTRODUCTION

Spatial Atomic Layer Deposition (s-ALD) is a high-throughput, chemical vapor deposition-like technique where a substrate is typically transported through a sequence of gases injected continuously at different locations.^{1,2} This sequenced exposure to reactant gases defines the ALD cycle that typically consists of precursor and coreactant dosing with two intermediate purge zones.

Within one ALD cycle, the growth of the material occurs through self-limiting half-reactions and, under the right temperature and dosing conditions, saturated growth is reached. This self-limiting nature of the growth enables precise thickness control, superior film quality, excellent uniformity on large-area substrates, and unparallel conformality over substrates having high aspect ratio structures.

Compared to conventional temporal ALD, spatial ALD offers the advantage of shorter cycle times which, in turn, determine higher throughput values. More specifically, in temporal ALD, a stationary substrate is exposed to time-sequenced gas pulses, and the separation of the precursor and coreactant is obtained by purge steps. For certain processes, these purge steps are several times longer than the typical reaction times, thus leading to long total cycle times that can limit the throughput.³ Instead, in *s*-ALD, the use of high flows of inert gases continuously fed to the substrate can virtually eliminate long purge steps, therefore shortening the total cycle time. This translates into higher throughput values, thus making *s*-ALD an attractive alternative for high-volume applications such as electronics, displays, photovoltaics, and batteries.^{4–6} These applications can benefit from *s*-ALD as they can make use of the key ALD merits while keeping the production costs fairly low. Furthermore, when a plasma is used as highly reactive coreactant in the so-called plasma-enhanced *s*-ALD (PE-*s*-ALD) approach, surface reactions can proceed at relatively low temperatures. This is advantageous as it allows depositions on temperature-sensitive substrates and it widens the available chemistry (e.g., in terms of precursors).⁷ As a result, more applications become feasible, including flexible devices requiring low-temperature processing.

PE-*s*-ALD can be performed at low pressure as well as at atmospheric pressure. Today, low-pressure PE-*s*-ALD is already used for high-volume manufacturing of semiconductor devices including state-of-the-art logic and memory.^{7–10} Instead, atmospheric-pressure PE-*s*-ALD is still in its infancy. For instance, besides our own work, PE-*s*-ALD of Al₂O₃ using trimethylaluminum [Al(CH₃)₃, TMA] and O₂ plasma has, so far, only been reported by Hoffmann *et al.*¹¹ and by Franke *et al.*¹² Furthermore, although exceptionally compatible with continuous mode operation such as sheet-to-sheet and roll-to-roll, only a few industrially relevant atmospheric-pressure PE-*s*-ALD processes have been developed so far.^{13–17} These research works mainly focus on demonstrating how atmospheric-pressure PE-*s*-ALD can be an enabling deposition technology for some of the aforementioned high-volume applications. Studies on the underlying chemistry of this class of processes are still largely lacking. Next to the development of novel deposition processes, gaining a better understanding of the growth mechanisms of the films and how they are influenced by the process parameters is vital to the advancement of this technology toward future applications.

Recently, we introduced a diagnostic approach based on the combination of infrared absorption spectroscopy on exhausted gases and optical emission spectroscopy (OES) on the plasma zone in order to study the chemistry of atmospheric-pressure PE-*s*-ALD processes.^{18,19} For the prototypical material Al₂O₃, this approach was demonstrated by investigating the plasma half-cycle when using TMA in combination with Ar–O₂ plasma at a temperature of 80 °C.¹⁸ The results were discussed in terms of combustion reactions of –CH₃ ligands at the surface (leading to CO₂ and H₂O reaction products) and thermal ALD-like ligand exchange reactions by H₂O produced as a combustion product (leading to CH₄ reaction products). In the present study, we have analyzed the process at more deposition temperatures (up to 200 °C) to gain more insight into this surface chemistry from the temperature-dependent trends of the reaction products created. Moreover, we report in more detail about the growth and film properties of the Al₂O₃ films as a

function of temperature. From the observations, we provide a refined growth mechanism and make a comparison with earlier results on temporal plasma-enhanced ALD of Al₂O₃.

II. EXPERIMENTAL SECTION

A. Reactor design

A schematic of the atmospheric-pressure PE-*s*-ALD reactor is presented in Fig. 1(a).¹⁹ A cylindrical reactor chamber is placed into a convection oven. The chamber consists of a fixed gas injection head and a rotating substrate table. In this configuration, the precursor and the coreactant are separated in space by a high flow of N₂ gas. Each reactant slot is provided with its own gas exhaust outlet. The N₂ flow in between and around the reactants acts as a purge medium and as a gas barrier isolating the process gases from ambient air.

A silicon wafer is placed on the rotating table at a distance of typically 20–250 μm from the reactant inlet slots. The exposure time of the substrate surface to the reactants is determined by the reactor geometry and the rotation speed. At a radial distance *r* from the center of the wafer, the exposure time to the precursor can be calculated as $t_{exp} = l/v$, where *l* is the width of the precursor slot (i.e., the width of the reaction zone where the precursor is dosed to the substrate surface) and *v* is the velocity of the substrate table. In the rotary lab-scale reactor, the velocity is defined by the rotation frequency expressed as number of rotations per minute (RPM). Therefore, longer exposures are achieved by rotating the substrate table at lower frequencies.

The atmospheric-pressure plasma used in the ALD experiments was generated by a Dielectric Barrier Discharge (DBD) plasma source. In a DBD source, the plasma is ignited between a high voltage (HV) electrode and a grounded electrode which are separated by a dielectric.²⁰ In the DBD source used for film deposition, alumina was used as the dielectric material. The plasma was ignited by means of a high voltage (HV) pulsed power supply, and the typical power density per dielectric barrier surface area is in the range 1–10 W/cm².^{13,14}

For the OES diagnostic study, a second dedicated DBD plasma source was used and its cross section is presented schematically in Fig. 1(b). In this design, the dielectric consists of a transparent quartz piece sandwiched between a grounded metal electrode and an HV voltage electrode. The grounded electrode is kept the same as in the previous configuration, whereas the HV top electrode is now made of a combination of silver and transparent conductive indium tin oxide (ITO). This specially designed DBD source provides a direct view on the substrate region through the transparent quartz/ITO configuration.

B. Film deposition and material characterization

Al₂O₃ films were deposited on 150-mm diameter silicon wafers at 80, 150, and 200 °C using TMA as the precursor and Ar–O₂ plasma as the coreactant. The TMA precursor was dosed to the reactor by using an Ar pick-up flow which is introduced into the precursor bubbler kept at room temperature. This pick-up flow through the bubbler is referred to as the TMA flow and was varied between 0.005 and 0.075 slm. Once leaving the bubbler, this flow is further diluted into Ar to reach a total flow of 1 slm which is transported to the chamber through heated lines. The coreactant

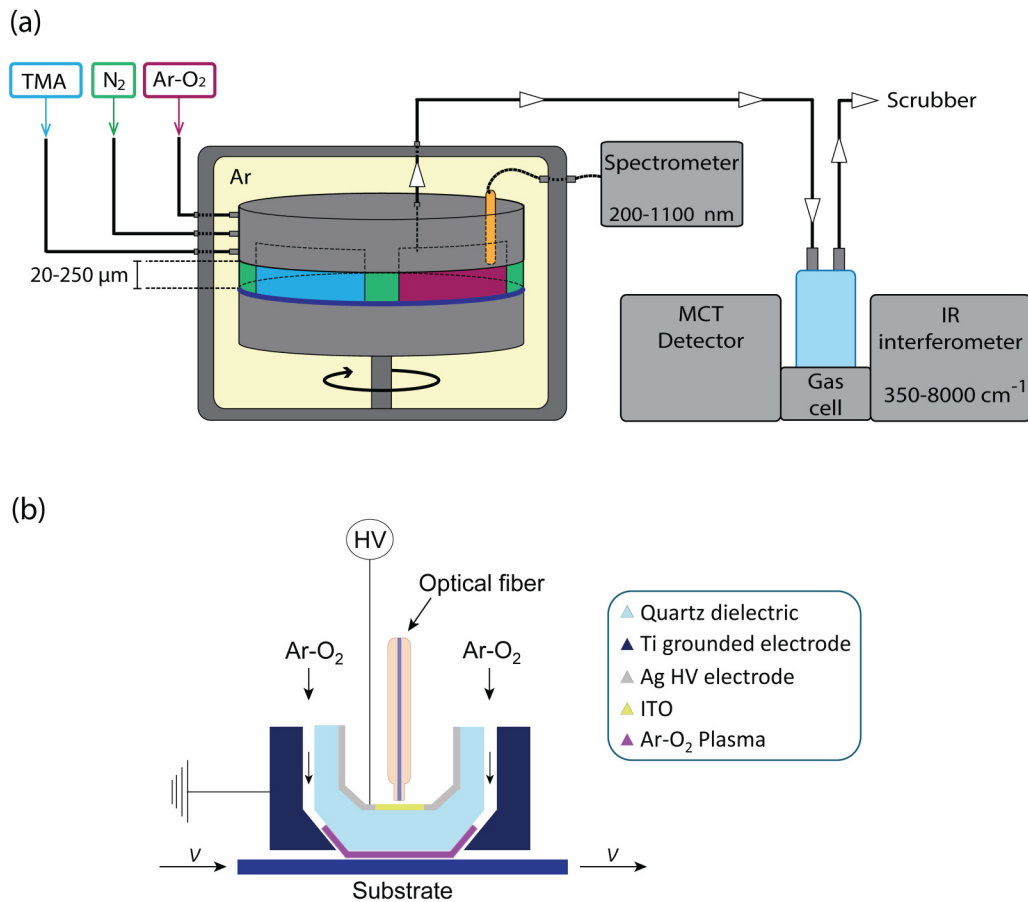


FIG. 1. Schematic of the diagnostic system implemented on the atmospheric-pressure PE-s-ALD reactor. (a) Gas-phase infrared spectroscopy of exhausted plasma gases and optical emission spectroscopy (OES) on the plasma-substrate region. (b) Cross section of the dedicated dielectric barrier discharge (DBD) plasma source providing the optical fiber with a direct view on the plasma-substrate region through a transparent indium tin oxide (ITO) top electrode and a quartz dielectric. While OES measurements are performed, the substrate moves with a velocity *v* underneath the plasma source.

mixture was kept constant using an O₂ flow of 0.08 slm and an Ar flow of 2.8 slm, reaching a concentration of 20% O₂ in Ar. Before each deposition, a step of 2 min of Ar-O₂ plasma was employed to clean the surface of the Si-wafer. Unless indicated otherwise, the substrate was rotated underneath the fixed gas injection head using a rotation frequency for the substrate table of 30 RPM. This frequency translates into an exposure time of the substrate surface to the precursor equal to 133 ms.

Thickness and refractive index of the as-deposited films were measured *ex situ* by spectroscopic ellipsometry (SE) using a J. A. Woollam M2000 spectrometer. A Cauchy optical model was used to fit the ellipsometry data and determine thickness and refractive index of the layers. From the thickness values, the GPC was calculated. The values of the refractive index are reported here at 632 nm (2 eV).

A combination of Rutherford Backscattering Spectroscopy (RBS) and Elastic Recoil Detection (ERD) was used to analyze the chemical composition of the alumina films. RBS and ERD were

performed by Detect99 using a Singletron system with a 3 MeV He⁺ beam. From the RBS/ERD results, the stoichiometry and the hydrogen content were obtained. The number of Al-atoms deposited per-cycle per nm² and mass density were calculated using the RBS/ERD and the SE data.

Fourier transform infrared (FTIR) spectroscopy was employed to further characterize the film composition. FTIR absorption measurements were carried out on 140 nm thick Al₂O₃ films deposited on silicon wafers. The absorbance spectra were obtained with a dry N₂-purged Bruker Tensor interferometer using a resolution of 6 cm⁻¹ and averaging the signal over ten scans. A bare silicon wafer was used to acquire a background spectrum for each sample.

C. Process diagnostics

Gas-phase infrared absorption spectroscopy was performed by means of a quartz gas-cell inserted into the sample compartment

of a Bruker VERTEX70 infrared interferometer. The exhausted plasma gas was fed into the gas-cell through of a stainless-steel line which was kept at room temperature. Before each experiment, the plasma line was flushed with 7 slm of N₂ to purge residual gases off the system. After achieving a stable background with only very small trace amounts of residual H₂O and CO₂ (indicating the purging is very effective to keep out gases from the atmosphere), a reference spectrum was acquired by flowing only N₂ through the plasma line. For each measurement, this reference spectrum is subtracted from the “ALD mode” spectrum. All infrared spectra of the exhaust plasma gas were recorded by using a collection time of 600 s at a resolution of 0.5 cm⁻¹.

OES was performed directly on the plasma-substrate region by using the home-built transparent DBD plasma source illustrated in Fig. 1(b) and described in Sec. II A. A thermally resistant optical fiber was inserted into the plasma source providing a direct view to the substrate through the Ar–O₂ plasma. To record the spectra, an Avantes spectrometer (AvaSpec-ULS2048 × 16) with a resolution of 0.5 nm was used. A background spectrum was acquired with no plasma ignition and subtracted from the “ALD mode” spectrum. During the OES analysis, a total integration time of 12 s was used for one single spectrum. The OES data presented in this work have been obtained by averaging the signal over a number of five recorded spectra. Likewise, the peak intensities reported here were calculated by averaging the values of the intensity over five spectra.

For both infrared and OES measurements, the spectra were acquired in “ALD mode,” where both TMA and plasma are activated on the substrate surface so that ALD reactions can occur and the gaseous reaction products can be identified (see the supplementary material⁴⁸).

III. RESULTS

A. Film growth and material characterization

Figure 2 shows the growth and compositional data for Al₂O₃ films of 140 nm thick deposited at 80, 150, and 200 °C using an exposure time of 133 ms and a bubbler flow of 0.075 slm. In our previous work,¹⁸ we reported that both ALD half-cycles show saturated growth when these processing conditions are used at a temperature of 80 °C. Therefore, it is plausible that for the same conditions, the growth will also be saturated at higher temperatures. Looking at the temperature dependence, Fig. 2 shows a clear decrease of the GPC in terms of thickness. A decrease is also present for the GPC in terms of Al-atoms deposited per nm² when going from 80 to 150 °C after which the GPC remained constant within the experimental accuracy. The mass density and refractive index slightly increase with temperature with the biggest effect again when going from 80 to 150 °C. In parallel, upon increasing the temperature, the H-content of the films largely decreases and the [O]/[Al] ratio approaches the value of 1.5 which corresponds to stoichiometric Al₂O₃.

Comparing our GPC data with those reported in the literature, we find that our GPC value of 0.18 nm obtained at 80 °C is in agreement with the value of 0.17 nm reported by Hoffmann *et al.* for a similar atmospheric-pressure PE-s-ALD process.¹¹ However, when comparing our results with the work by Potts *et al.*²¹ for the low-pressure temporal PE-ALD case, we find somewhat higher

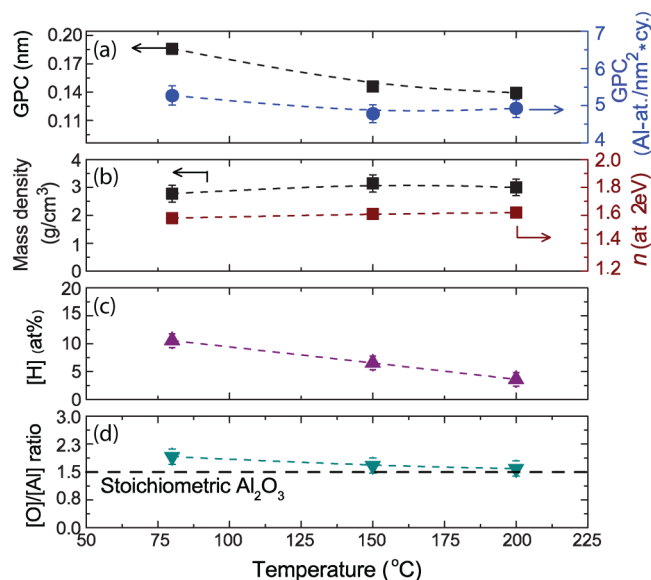


FIG. 2. Growth and compositional data for the Al₂O₃ films deposited at 80, 150, and 200 °C. For each temperature, an exposure time of 133 ms and a TMA flow of 0.075 slm were used. (a) Growth-per-cycle (GPC) in terms of thickness and Al-atoms deposited per nm² as obtained by SE and RBS, respectively; (b) mass density and refractive index as measured RBS and SE; (c) H-concentration as measured by ERD; and (d) [O]/[Al] ratio as measured by RBS.

GPC values (see Fig. S1 in the supplementary material⁴⁸). This difference is potentially due to the difference in operating pressure (compare, e.g., the dependence of the GPC of Al₂O₃ on the H₂O flow rate even when working under saturation conditions),²² but the exact reason is not yet clear.

The trend of a decreasing GPC with increasing temperature is in good agreement with previous reports for low-pressure ALD of Al₂O₃ where both O₂ plasma and O₃ were used as coreactants. For the low-pressure PE-ALD, Potts *et al.* observed a decrease in GPC and improved material characteristics within the temperature range between 25 and 300 °C.²¹ The same trend was found by Kim *et al.* using O₃ as the coreactant.²³ It is well accepted that the decrease of GPC with temperature is largely due to thermally activated dehydroxylation reactions which induce a lower density of –OH surface sites. This leads to a lower density of adsorption sites for TMA and hence to less TMA adsorption on the surface.²⁴ This manifests in a decrease of Al-atoms deposited per nm², as particular seen between 80 and 150 °C in Fig. 2(a).

In terms of material composition,¹⁸ the mass density and refractive index values found here are in agreement with the ones reported in the literature for the low-pressure PE-ALD case.^{25,26} The mass density increases from 2.7 g/cm³ at 80 °C to 3.0 g/cm³ at 200 °C. This increase leads to a larger change in GPC in terms of thickness compared to the GPC in terms of Al-atoms per nm². Furthermore, the increase in density is accompanied by a reduction of the H-content in the film from 10 at. % to less than 5 at. %. This

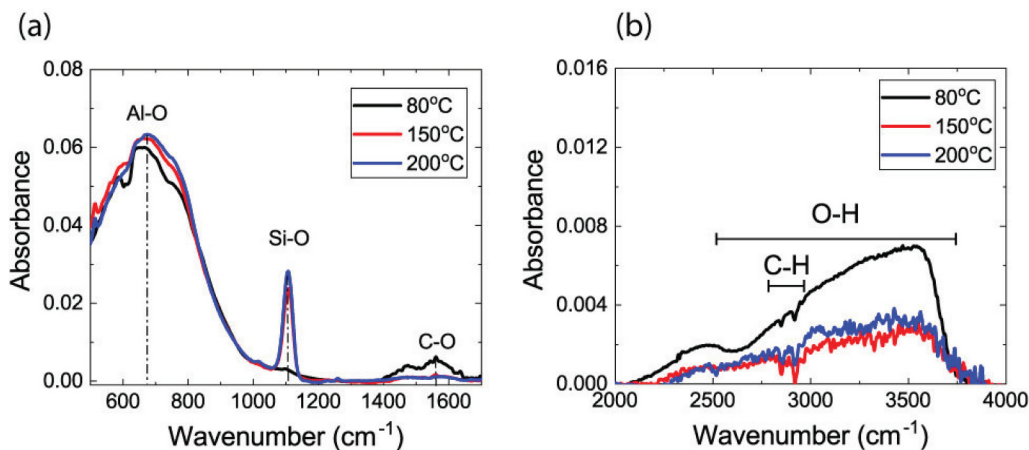


FIG. 3. Infrared absorbance spectra in the two wavenumber regions of interest for the Al_2O_3 films deposited by PE-s-ALD at 80, 150, and 200 °C: (a) 500–1700 and (b) 2000–4000 cm^{-1} .

effect, together with the decrease in $[\text{O}]/[\text{Al}]$ ratio from 1.9 at 80 °C to 1.5 at 200 °C, suggests that at higher temperatures less $-\text{OH}$ groups are incorporated in the films as has also been observed by infrared spectroscopy measurements discussed below.

To further investigate the composition of the deposited layers, infrared absorption spectroscopy was carried out on the Al_2O_3 films. The results are shown in Fig. 3, and the assignment of the vibrational modes is listed in Table I. The broad peak in the region between 500 and 1000 cm^{-1} is attributed to the Al–O stretching mode and it slightly increases with temperature. This increase was also observed for Al_2O_3 layers prepared by PE-ALD and indicates that more Al–O bonds are created at higher temperatures.²⁷ The intensity of the peak at 1050 cm^{-1} (indicative for the Si–O rocking mode) indicates that the interfacial SiO_x layer between the Si-wafer and the Al_2O_3 film, as is commonly observed,²⁷ is slightly thicker at elevated temperatures. The feature in the region 1400–1700 cm^{-1} is assigned to C–O vibrations which can be related to the presence of formate (COOH^-) and carbonate (CO_3^{2-}) groups in the film.^{27–29} The decrease with temperature of these modes implies that less of these carbonaceous species are incorporated in the films when working at higher temperatures. The decreasing intensity of the broad O–H stretching mode at 2600–3800 cm^{-1} at higher deposition temperatures suggests that these films contain less $-\text{OH}$

groups due to thermally activated dihydroxylation reactions. Superimposed on the broad O–H stretching mode, there is a contribution from the C–H stretching mode at 2900–3100 cm^{-1} , which can be due to the incorporation of $-\text{CH}_x$ groups in the films. Overall, the data in Fig. 3 are in line with the RBS/ERD data in Fig. 2 showing lower H-content and improved stoichiometry at high temperatures.

B. Gas-phase infrared spectroscopy

To identify the species produced in the plasma half-cycles, the gases in the plasma exhaust were analyzed by infrared spectroscopy. In Fig. 4, the data are given for each deposition temperature. The absorbance peaks corresponding to O_3 , CH_3OH , CO , CO_2 , CH_4 , CH_2O , and H_2O species were observed with the assignments of vibrational modes listed in Table II.

The detected O_3 is produced in the atmospheric-pressure O_2 plasma indifferent from the ALD reactions. The other species are formed in surface and gas-phase reactions during the removal of $-\text{CH}_3$ ligands from the surface in the ALD cycle.¹⁸ Figure 4 shows that the magnitude of absorbance by O_3 , CO_2 , CH_4 , and CH_2O is affected by the deposition temperature. A large effect is seen for the absorbance of O_3 which strongly reduces with increasing temperature. The absorbance for CO_2 slightly decreases with increasing temperature whereas the absorbance for H_2O shows no clear trend with temperature. The absorbances for CH_4 and CH_2O show an increasing trend. In particular, CO_2 and CH_4 show opposite temperature trends which suggest that these species originate from different reaction pathways.

To study surface saturation, infrared spectra were taken at the three deposition temperatures for different TMA flows. The surface saturation can be investigated by evaluating the integrated area of the absorbance peaks for the most relevant species.¹⁸ Figure 5 depicts the integrated peak areas for CO_2 , H_2O , CH_4 , and CH_2O as a function of the TMA flow. At each temperature, the densities of

TABLE I. Infrared vibrational modes and their peak positions in the infrared spectra as measured for the Al_2O_3 films.

Vibrational mode	Wavenumber range (cm^{-1})	Reference
Al–O stretching	500–1000	27
Si–O rocking	1050	27
C–O stretching	1400–1700	27–29
C–H stretching	2900–3100	27
O–H stretching	2600–3800	27

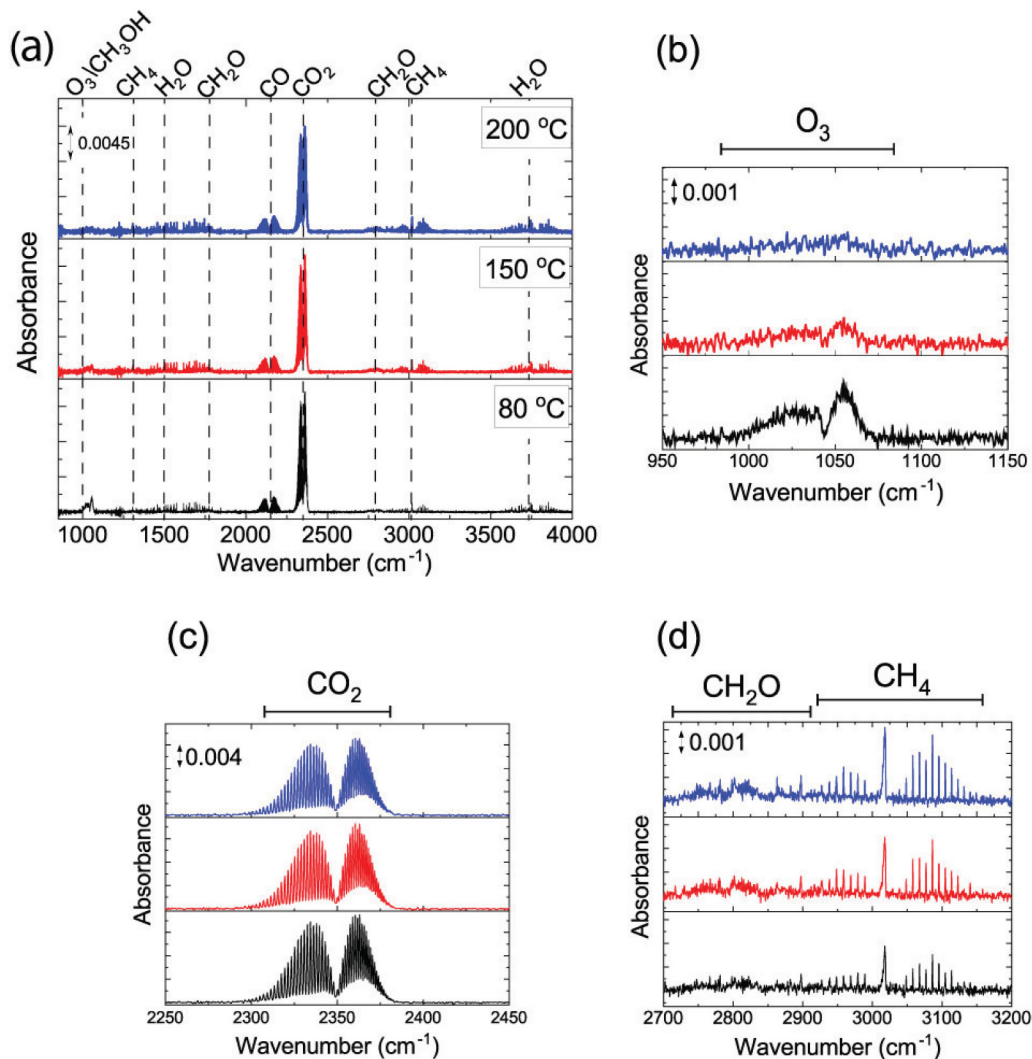


FIG. 4. Gas-phase infrared absorption spectra of the exhausted plasma gases during growth of Al_2O_3 in ALD mode at 80, 150, and 200 °C (a). Zoomed-in view for (b) O_3 , (c) CO_2 , and (d) $\text{CH}_4/\text{CH}_2\text{O}$ absorbance spectra. For each temperature, an exposure time of 133 ms and a TMA flow of 0.075 slm were used.

all components show saturated behavior at a TMA flow of 0.035 slm, meaning that this flow is sufficient to saturate the surface with precursor molecules.

In addition to the saturation behavior, Fig. 5 can also provide further insights into the influence of temperature on the reaction mechanism. A comparison of the absorbance values for different deposition temperatures shows that, although CO_2 and H_2O are both combustion products, their absorbance values exhibit different temperature-dependent behaviors. Specifically, CO_2 absorbance decreases with temperature pointing to a decrease of combustion reactions at higher temperatures whereas the H_2O absorbance does not show a clear temperature trend. The H_2O absorbance appears to be similar for 80 and 200 °C while it is somewhat lower

for 150 °C. The absorbance values of CH_4 and CH_2O exhibit an increase with temperature when going from 80 to 200 °C.

C. Optical emission spectroscopy

To gain insight into the nature and behavior of the excited plasma species, we carried out OES studies directly on the region where the plasma interacts with the substrate. In the spectral range between 300 and 600 nm, we identified the emission bands of OH at 309 nm ($A^2\Sigma^+ \rightarrow X^2\Pi$) and CH at 389 nm ($B^2\Sigma \rightarrow X^2\Pi$) and at 431 nm ($A^2\Delta \rightarrow X^2\Pi$) ($b^4\Sigma_g^- \rightarrow a^4\Pi_u$). Furthermore, the emission from Ar at 415–426 nm ($5p \rightarrow 4s$) and the first negative system (FNS) of O_2^+ at 557.8 nm were observed.

TABLE II. Infrared vibrational modes with assigned species and (main) peak position in the gas-phase infrared spectra measured on the exhaust plasma gas. The assignments are based on the gas-phase infrared spectra of the listed species as reported in the NIST database.³⁰

Species	Vibrational mode	Wavenumber peak position (cm ⁻¹)
O ₃	Asymmetric stretching	1040
CH ₃ OH	C–O stretching	1033
CH ₄	Degenerate deformation	1306
H ₂ O	Bending	1594
CH ₂ O	C–O stretching	1746
CO	Stretching	2143
CO ₂	Asymmetric stretching	2349
CH ₂ O	C–H symmetric stretching	2782
CH ₄	Degenerate stretching	3018
H ₂ O	Asymmetric stretching	3756

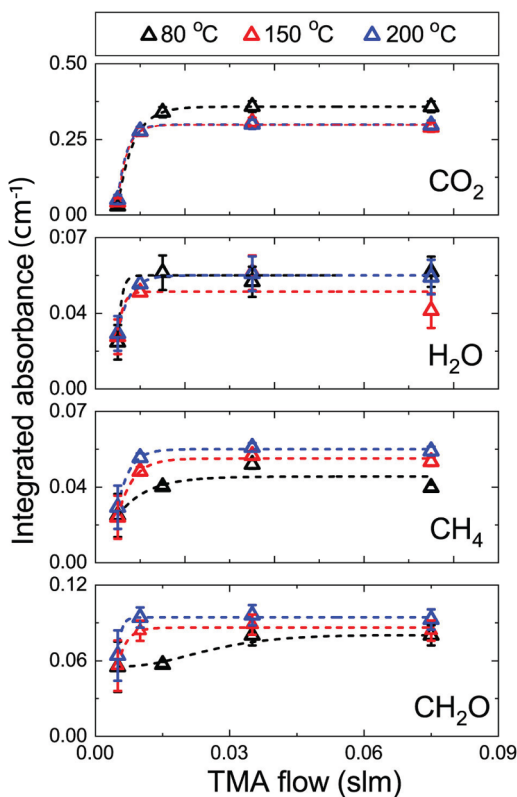


FIG. 5. Integrated infrared absorbance peaks of CO₂ (2349 cm⁻¹), H₂O (3656 cm⁻¹), CH₄ (3018 cm⁻¹), and CH₂O (2782 cm⁻¹) as a function of the TMA flow during Al₂O₃ growth at 80, 150, and 200 °C, respectively, and using an exposure time of 133 ms. The dashed lines serve as a guide to the eye.

Figure 6(a) shows parts of the OES spectra corresponding to a TMA flow of 0.075 slm. The emission from excited OH and CH species indicates the presence of reaction products in the plasma, while the Ar and O₂⁺ lines are characteristic for the emission spectrum of the Ar–O₂ plasma. More specifically, the OH and CH excited fragments are produced by electron collisions in the plasma involving reaction products from the surface. Most likely, the OH emission originates from electron-induced dissociative excitation of H₂O molecules,³¹

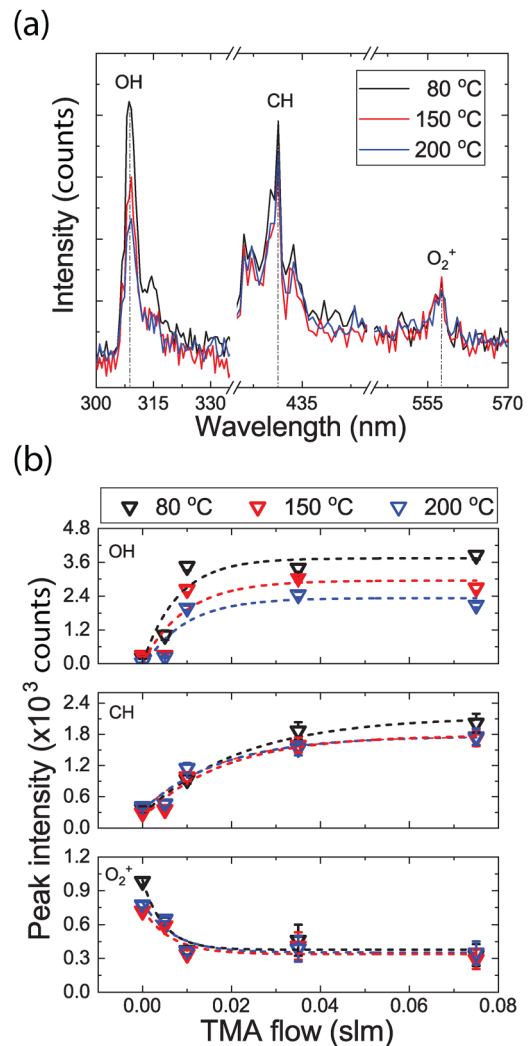
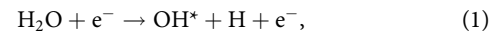


FIG. 6. OES results for PE-s-ALD of Al₂O₃ at 80, 150, and 200 °C. (a) OES emission spectrum in ALD mode obtained at a TMA flow of 0.075 slm and an exposure time of 133 ms. (b) Peak intensity of OH, CH, and O₂⁺ emission lines as a function of the TMA flow. The dashed lines serve as a guide to the eye.

with OH* indicated electronically excited OH. The CH emission can originate from similar dissociative excitation reactions of species such as CH₄, CH₂O, and CH₃OH which are also reaction products of the surface reactions.^{32,33} Figure 6(a) shows that the intensity of the OH emission band decreases with temperature, thus pointing to a lower content of H₂O in the plasma. The CH emission remains roughly constant but this trend cannot simply be assigned to one of the reaction products. The O₂⁺ emission band remains largely constant indicating that the plasma is not affected significantly by the temperature change.

Figure 6(b) shows the peak intensities for the OH, CH, and O₂⁺ emission lines as a function of the precursor flow. Similar to the case of the infrared data in Fig. 5, the peak intensity of the OH and CH emission bands indicates that saturation is reached at a TMA flow of 0.035 slm for each deposition temperature. Conversely, the intensity of the O₂⁺ peak decreases with increasing TMA flows and reaches a saturated value at 0.01 slm.

Comparing the results presented in Fig. 6 with those in Fig. 5 shows that the decrease of the OH emission—attributed to a decrease in H₂O—behaves somewhat different from the H₂O absorbance which does not show a clear trend with temperature. On the other hand, it does agree with the decrease of the CO₂ absorbance when considering that H₂O and CO₂ are both combustion products. Therefore, we hypothesize that the fact that the H₂O absorbance does not show a clear dependence with temperature is due to a reduced sensitivity of this measurement for trends with temperature (H₂O can easily accumulate in the system and is harder to purge). The fact that the CH emission does not show a clear trend with temperature—different from the CH₄ absorbance—might indicate that the CH emission is only due to CH₄ but potentially also due to CH₂O and CH₃OH.

IV. DISCUSSION

The results of the plasma half-cycle investigation presented in Sec. III can clarify how the deposition temperature affects the underlying chemistry of the atmospheric-pressure PE-s-ALD process of Al₂O₃. On the base of our observations, we will now discuss a refinement of the growth mechanism that was proposed in our earlier work for PE-s-ALD.¹⁸

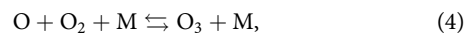
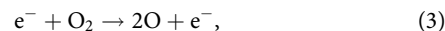
During the precursor step, TMA molecules adsorb on the surface in their reaction with –OH surface groups and the first half-cycle can be described by the following reaction:



Here, –CH₃ ligands are protonated to volatile CH₄ molecules and, at the end of the precursor step, the surface will be covered with the adsorbed TMA fragments with their remaining unreacted –CH₃ ligands. In Reaction (2), we have assumed that TMA adsorbs monofunctionally, i.e., through the exchange of one –CH₃ ligand, but bifunctional adsorption can also occur.³⁴ Upon a temperature increase, dehydroxylation reactions cause two adjacent –OH groups to react and leave the surface as a H₂O molecule. As a result, at higher temperatures, there is a reduced density of –OH surface groups acting as reactive sites for the incoming TMA molecules, thus leading to less precursor adsorption.^{23,26,34} This is particularly

clear from the Al-atoms deposited per nm² when increasing the temperature from 80 to 150 °C [Fig. 2(a)].

For the plasma half-cycle, the infrared spectra on the exhaust plasma gas have shown the presence of O₃ in the Ar–O₂ plasma. This is in line with the fact that O₃ is naturally produced in atmospheric-pressure O₂ plasmas due to following reaction sequence:^{20,35–37}

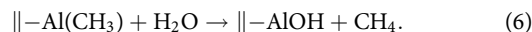


with M in the temperature three-body reaction most likely being O₂ and Ar. As a consequence, the Ar–O₂ plasma coreactant in our conditions is a mixture composed of O₂ plasma species such as O-atoms as well as O₃. Both types of species can take part in the ligands removal through combustion-like reactions.^{29,31,38,39} In particular, O₃ reacts with the surface by decomposing into O₂ and O which will then initiate the surface reactions.⁴⁰ Such decomposition reactions can happen at any surface and not just under ALD conditions through three-step dissociative reactions.^{41,42} For Al₂O₃ surfaces, Knoops *et al.* showed that the O₃ surface recombination probability is rather low and that this value does not vary much with temperature within the range 100–200 °C.⁴³ Hence, the decreasing trend of O₃ absorbance with increasing temperature might be largely due to ALD surface reactions or less O₃ is effectively produced at higher temperatures through reaction (4).³⁷

Assuming that O-atoms from the O₂ plasma as well as from O₃ dissociation are involved in the surface chemistry during the coreactant half-cycle, the O-atoms react with the methylated surface by insertion into the Al–C bonds. The removal of the –CH₃ ligands is then driven by combustion reactions that lead to the production of CO₂ and H₂O according to



Moreover, H₂O that has desorbed in these combustion-like reactions can react with the surrounding –CH₃ ligands in a thermal ALD-like pathway according to

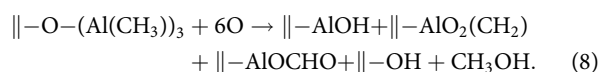


Both the combustion byproducts (CO₂ and H₂O) and the thermal ALD-like byproduct, CH₄ are identified in the infrared spectrum of the second half-cycle (Fig. 4), thus indicating that the reaction mechanism is characterized by the coexistence of these two reaction pathways. This indication is further confirmed by the fact that the temperature increase affects the combustion and thermal reaction pathways in different ways. On one side, thermally activated dehydroxylation causes a lower –OH density leading to a lower TMA uptake. As a consequence, at higher temperatures, less –CH₃ ligands are available on the surface as adsorbates for subsequent O-activated reactions, and, therefore, the production of combustion byproducts decreases with temperature.^{34,44} This is demonstrated by the decrease of CO₂ absorbance and OH emission [Fig. 6(b)] with temperature. In particular, OH emission originates from electron-induced dissociative excitation of H₂O molecules

[Reaction (1)] that are formed in the ligand combustion. Hence, the decrease of OH emission confirms that less H₂O is produced through combustion at higher temperature.³¹ The fact that the H₂O absorbance in Fig. 5 does not show a clear dependence with temperature might be due to a reduced sensitivity of this measurement for the temperature trend as discussed in Sec. III C.

On the other hand, the thermal ALD reaction (6) becomes more relevant at higher temperatures and leads to more CH₄ as concluded from the absorbance data in Fig. 5. For the thermal ALD process of TMA and H₂O, the reaction kinetics study by Vandalon and Kessels showed that the reaction cross section of H₂O to -CH₃ increases with temperature.⁴⁵

Infrared spectra also show the absorbance from CH₂O and CH₃OH, two products not yet experimentally reported for PE-ALD of Al₂O₃. A Density Functional Theory (DFT) study by Fomengia *et al.* has predicted these species to be formed from reactions of TMA with both O₂ plasma and O₃. In that work, the following reactions have been reported under saturation conditions:^{18,39}



As these species have not been observed in the studies of the low-pressure PE-ALD case, we speculate that the use of an atmospheric-pressure plasma with a higher density of O-atoms may create conditions favorable to the formation of these species. In addition to surface reactions, it is also possible that these CH-containing species are produced in gas-phase reactions occurring in the plasma. These gas-phase reactions can start with CH₄ released into the plasma due to the thermal ALD-like reactions.^{32,46,47} The fact that more thermal ALD-like reactions occur at higher temperatures producing more CH₄ is in line with the increased intensity of CH₂O at higher temperatures. Yet, the presence of reactions (7) and (8) can certainly not be excluded.

V. CONCLUSIONS

The atmospheric-pressure PE-s-ALD deposition process of Al₂O₃ from TMA and Ar-O₂ plasma was investigated with a combination of thin-film and gas-phase spectroscopic diagnostic techniques within the temperature range from 80 to 200 °C. The thin-film analysis revealed insight into the temperature dependence of the growth-per-cycle (GPC) and film composition, and a comparison with the low-pressure case of PE-ALD of Al₂O₃ was made. The combination of infrared absorbance spectroscopy and optical emission spectroscopy diagnostics was used to identify the gas-phase species involved in the underlying chemistry of the plasma half-cycle. The production of these species was studied as a function of the precursor flow and processing temperature.

These investigations allowed to identify those process conditions giving surface saturation and to gain insight into the growth mechanism. By studying the produced byproducts as a function of temperature, we found that the -CH₃ ligands are removed by both combustion reactions and thermal ALD-like reactions. The combustion reactions are initiated by the O₂ plasma species yielding

CO₂ and H₂O, whereas the thermal reactions are initiated by H₂O molecules and result into CH₄ production. These two reaction pathways are affected differently by the temperature change. Upon a temperature increase, thermal dehydroxylation causes a lower density of -OH sites yielding less TMA adsorption. In turn, less -CH₃ ligands are available to be combusted to CO₂ and H₂O at higher temperatures. At the same time, the increased reactivity of H₂O at higher temperatures favors the activation of more thermal ALD-like reactions such that more CH₄ is formed. This CH₄ can undergo further gas-phase dissociation in the plasma to form CH₂O although surface chemical reactions are also possible during ALD.

The reaction mechanism proposed for the PE-s-ALD process of Al₂O₃ appears to be very similar to the reaction mechanism for temporal PE-ALD at low pressures although for the earlier investigations no temperature dependence for the production of reaction products was available. The current study provides, therefore, additional insight. Moreover, the role of O₃ might be smaller for PE-ALD at low pressures as the production of O₃ is enhanced at higher temperatures. Another difference is that we have clearly observed CH₃OH and CH₂O in this work. These species were not observed in the low-pressure case which can imply an influence of the atmospheric pressure although it could also be due to an enhanced sensitivity of the diagnostic approach applied.

Finally, we want to highlight that this complementary spectroscopy diagnostic approach can also be employed to study other materials and processes, thus, expanding the fundamental knowledge existing on atmospheric-pressure PE-s-ALD and contributing to further advancement of this emerging technique.

ACKNOWLEDGMENTS

The authors would like to acknowledge the Material Innovation Institute M2i, the Netherlands Organization for Scientific Research NWO, and the Netherlands Organization for Applied Scientific Research TNO (Holst Centre) for their financial support (NWO-M2i Contract No. F61.4.15561). The authors acknowledge the help provided by F. Grob for the help provided at the ALD reactor. Finally, we acknowledge Y. Creighton for his contribution to the plasma source design.

AUTHOR DECLARATIONS

Conflict of Interest

The authors have no conflicts to disclose.

Author Contributions

M. A. Mione: Conceptualization (equal); Data curation (equal); Formal analysis (equal); Investigation (equal); Methodology (equal); Writing – original draft (equal); Writing – review & editing (equal). **V. Vandalon:** Conceptualization (supporting); Investigation (supporting). **W. M. M. Kessels:** Conceptualization (equal); Writing – original draft (equal); Writing – review & editing (equal). **F. Roozeboom:** Funding acquisition (equal); Supervision (equal); Writing – original draft (equal).

DATA AVAILABILITY

The data that support the findings of this study are available within the article and its supplementary material.

REFERENCES

- ¹P. Poodt, D. C. Cameron, E. Dickey, S. M. George, V. Kuznetsov, G. N. Parsons, F. Roozeboom, G. Sundaram, and A. Vermeer, *J. Vac. Sci. Technol. A* **30**, 010802 (2012).
- ²D. Muñoz-Rojas, V. Huong Nguyen, C. Masse de la Huerta, C. Jiménez, and D. Bellet, "Spatial atomic layer deposition," in *Chemical Vapor Deposition for Nanotechnology*, edited by P. Mandracci (IntechOpen, London, 2019), pp 3–27, ISBN 978-1-78984-960-8.
- ³A. W. Ott, J. W. Klaus, J. M. Johnson, and S. M. George, *Thin Solid Films* **292**, 135 (1997).
- ⁴J. Sun *et al.*, *IEEE Electron Device Lett.* **29**, 721 (2008).
- ⁵A. Illiberi, F. Roozeboom, and P. Poodt, *ACS Appl. Mater. Interfaces* **4**, 268 (2012).
- ⁶D. H. Levy, D. Freeman, S. F. Nelson, P. J. Cowdery-Corvan, and L. M. Irving, *Appl. Phys. Lett.* **92**, 192101 (2008).
- ⁷H. C. M. Knoops, T. Faraz, K. Arts, and W. M. M. Kessels, *J. Vac. Sci. Technol. A* **37**, 030902 (2019).
- ⁸TEL, <https://www.tel.com/product/nt333.html> (accessed 12 August 2022).
- ⁹Wonik IPS, <http://www.ips.co.kr/en> (accessed 12 August 2022).
- ¹⁰AMAT, <https://publish-p33711-e119406.adobecloud.com/content/applied-materials/us/en/product-library/olympia-ald> (accessed 12 August 2022).
- ¹¹L. Hoffmann *et al.*, *ACS Appl. Mater. Interfaces* **9**, 4171 (2017).
- ¹²S. Franke *et al.*, *J. Vac. Sci. Technol. A* **35**, 01B117 (2017).
- ¹³Y. Creighton, A. Illiberi, M. A. Mione, W. van Boekel, N. Debernardi, M. Seitz, and F. Roozeboom, *ECS Trans.* **75**, 11 (2016).
- ¹⁴F. J. van den Bruele, M. Smets, A. Illiberi, Y. Creighton, P. Buskens, F. Roozeboom, and P. Poodt, *J. Vac. Sci. Technol. A* **33**, 01A131 (2015).
- ¹⁵M. A. Mione, I. Katsouras, Y. Creighton, W. van Boekel, J. Maas, G. Gelinck, F. Roozeboom, and A. Illiberi, *ECS J. Solid State Sci. Technol.* **6**, N243 (2017).
- ¹⁶L. Hoffmann *et al.*, *J. Vac. Sci. Technol. A* **36**, 01A112 (2018).
- ¹⁷L. Hoffmann, K. O. Brinkmann, J. Malerczyk, D. Rogalla, T. Becker, D. Theirich, I. Shutsko, P. Görrn, and T. Riedl, *ACS Appl. Mater. Interfaces* **10**, 6006 (2018).
- ¹⁸M. A. Mione, R. Engel, V. Vandalon, W. M. M. Kessels, and F. Roozeboom, *Appl. Phys. Lett.* **115**, 083101 (2019).
- ¹⁹M. A. Mione, V. Vandalon, A. Mameli, W. M. M. Kessels, and F. Roozeboom, *J. Phys. Chem. C* **125**, 24945 (2021).
- ²⁰U. Kogelschatz, *Plasma Chem. Plasma Process.* **23**, 1 (2003).
- ²¹S. E. Potts, W. Keuning, E. Langereis, G. Dingemans, M. C. M. van de Sanden, and W. M. M. Kessels, *J. Electrochem. Soc.* **157**, P66 (2010).
- ²²R. Matero, A. Rahtu, M. Ritala, M. Leskelä, and T. Sajavaara, *Thin Solid Films* **368**, 1 (2000).
- ²³S. K. Kim, S. W. Lee, C. S. Hwang, Y.-S. Min, J. Y. Won, and J. Jeong, *J. Electrochem. Soc.* **153**, F69 (2006).
- ²⁴C. E. Nelson, J. W. Elam, M. A. Cameron, M. A. Tolbert, and S. M. George, *Surf. Sci.* **416**, 341 (1998).
- ²⁵M. D. Groner, F. H. Fabreguette, J. W. Elam, and S. M. George, *Chem. Mater.* **16**, 639 (2004).
- ²⁶E. Langereis, M. Bouman, J. Keijmel, S. Heil, M. C. M. van de Sanden, and W. M. M. Kessels, *ECS Trans.* **16**, 247 (2008).
- ²⁷V. Verlaan, L. R. J. G. van den Elzen, G. Dingemans, M. C. M. van de Sanden, and W. M. M. Kessels, *Phys. Status Solidi Curr. Top. Solid State Phys.* **7**, 976 (2010).
- ²⁸V. R. Rai, V. Vandalon, and S. Agarwal, *Langmuir* **28**, 350 (2012).
- ²⁹D. N. Goldstein, J. A. McCormick, and S. M. George, *J. Phys. Chem. C* **112**, 19530 (2008).
- ³⁰NIST Chemistry WebBook, <https://webbook.nist.gov/chemistry/> (accessed 5 July 2021).
- ³¹S. B. S. Heil, J. L. van Hemmen, M. C. M. van de Sanden, and W. M. M. Kessels, *J. Appl. Phys.* **103**, 103302 (2008).
- ³²R. J. H. Klein-Douwel, J. Luque, J. B. Jeffries, G. P. Smith, and D. R. Crosley, *Appl. Opt.* **39**, 3712 (2000).
- ³³M. C. Branch, M. E. Sadequ, A. A. Alfarayedhi, and P. J. Van Tiggelen, *Combust. Flame* **83**, 228 (1991).
- ³⁴E. Langereis, J. Keijmel, M. C. M. van de Sanden, and W. M. M. Kessels, *Appl. Phys. Lett.* **92**, 231904 (2008).
- ³⁵A. Schütze, J. Y. Jeong, S. E. Babayan, J. Park, G. S. Selwyn, and R. F. Hicks, *IEEE Trans. Plasma Sci.* **26**, 1685 (1998).
- ³⁶B. Eliasson, M. Hirth, and U. Kogelschatz, *J. Phys. D: Appl. Phys.* **20**, 1421 (1987).
- ³⁷S. W. Benson and A. E. Axworthy, *J. Chem. Phys.* **26**, 1718 (1957).
- ³⁸V. R. Rai, V. Vandalon, and S. Agarwal, *Langmuir* **26**, 13732 (2010).
- ³⁹G. N. Fomengia, M. Nolan, and S. D. Elliott, *Phys. Chem. Chem. Phys.* **20**, 22783 (2018).
- ⁴⁰S. D. Elliott, G. Scarel, C. Wiemer, M. Fanciulli, and G. Pavia, *Chem. Mater.* **18**, 3764 (2006).
- ⁴¹W. Li, G. V. Gibbs, and S. T. Oyama, *J. Am. Chem. Soc.* **120**, 9041 (1998).
- ⁴²S. T. Oyama, *Catal. Rev.* **42**, 279 (2000).
- ⁴³H. C. M. Knoops, J. W. Elam, J. A. Libera, and W. M. M. Kessels, *Chem. Mater.* **23**, 2381 (2011).
- ⁴⁴A. Rahtu, T. Alaranta, and M. Ritala, *Langmuir* **17**, 6506 (2001).
- ⁴⁵V. Vandalon and W. M. M. Kessels, *Appl. Phys. Lett.* **108**, 011607 (2016).
- ⁴⁶A. Indarto, J. W. Choi, H. Lee, and H. K. Song, *Chinese Sci. Bull.* **53**, 2783 (2008).
- ⁴⁷L. Wang, Y. Yi, H. Guo, and X. Tu, *ACS Catal.* **8**, 90 (2018).
- ⁴⁸See the supplementary material at <https://www.scitation.org/doi/suppl/10.1116/6.0002158> for the method used to analyze the infrared and OES spectra.